



# Establishment of a Lung Metastatic Breast Tumor Xenograft Model in Nude Rats

Joris Tchouala Nofiele<sup>1,2</sup>, Hai-Ling Margaret Cheng<sup>1,2,3,4\*</sup>

**1** The Research Institute and Diagnostic Imaging, Hospital for Sick Children, Toronto, Ontario, Canada, **2** Department of Medical Biophysics, University of Toronto, Toronto, Ontario, Canada, **3** Leslie Dan Faculty of Pharmacy, University of Toronto, Toronto, Ontario, Canada, **4** The Institute of Biomaterials & Biomedical Engineering, University of Toronto, Toronto, Ontario, Canada

## Abstract

**Objective:** Larger animal models provide relevant tumor burden in the development of advanced clinical imaging methods for non-invasive cancer detection and diagnosis, and are especially valuable for studying metastatic disease. Most available experimental models, however, are based on immune-compromised mice. To lay the foundation for studying spontaneous metastasis using non-invasive magnetic resonance imaging (MRI), this study aims to establish a highly metastatic breast cancer xenograft model in nude rats.

**Materials and Methods:** A highly metastatic variant of human adenocarcinoma MDA-MB-231 known as LM2 was inoculated into nude rats. Orthotopic and subcutaneous (flank) sites were compared, with half of the orthotopic injections guided by ultrasound imaging. MRI with gadolinium contrast administration was performed weekly beginning on Day 6 and ending on Day 104. Excised tumors were assessed on histology using hematoxylin and eosin and CD34. Fisher's exact test was used to compare successful tumor induction amongst different inoculation methods.

**Results:** Primary LM2 tumors were established orthotopically in all cases under ultrasound-guided injection, and none otherwise ( $p=0.0028$ ). Contrast-enhanced MRI revealed rapidly progressing tumors that reached critical size (15 mm diameter) in 2 to 3 weeks after inoculation. MRI and histology findings were consistent: LM2 tumors were characterized by low vascularity confined to the tumor rim and large necrotic cores with increasing interstitial fluid pressure.

**Conclusions:** The metastatic LM2 breast tumor model was successfully established in the mammary fat pads of nude rats, using ultrasound needle guidance as a non-invasive alternative to surgery. This platform lays the foundation for future development and application of MRI to study spontaneous metastasis and different stages throughout the metastatic cascade.

**Citation:** Nofiele JT, Cheng H-LM (2014) Establishment of a Lung Metastatic Breast Tumor Xenograft Model in Nude Rats. PLoS ONE 9(5): e97950. doi:10.1371/journal.pone.0097950

**Editor:** Lu-Zhe Sun, University of Texas Health Science Center, United States of America

**Received:** February 5, 2014; **Accepted:** April 26, 2014; **Published:** May 16, 2014

**Copyright:** © 2014 Nofiele, Cheng. This is an open-access article distributed under the terms of the Creative Commons Attribution License, which permits unrestricted use, distribution, and reproduction in any medium, provided the original author and source are credited.

**Funding:** This study was supported by funding from the Natural Sciences and Engineering Research Council of Canada (#355795) and the Garron Family Cancer Centre Grant through the SickKids Foundation. The funders had no role in study design, data collection and analysis, decision to publish, or preparation of the manuscript.

**Competing Interests:** The authors have declared that no competing interests exist.

\* E-mail: hailing.cheng@utoronto.ca

## Introduction

Current medical imaging technologies play a critical role in the diagnosis and management of cancer patients. Magnetic resonance imaging (MRI), for example, is a non-irradiative whole-body imaging platform that enables accurate localization and sensitive delineation of tumor masses, characterization of tumor vascularity, and non-invasive monitoring of treatment effects [1–3]. Imaging also plays a key role in the clinical translation of new treatment paradigms, as a non-invasive method is ultimately desired for monitoring the progress of patients receiving therapy. However, imaging technologies that are used to test the efficacy and safety of new investigational drugs in preclinical mouse models are not easily translated to human imaging. In other words, there is a gap in the technologies developed for preclinical testing and those ultimately required in the clinic. One way to close this gap is to use larger animal models. Not only can larger animals be

imaged at spatial resolutions easily translated to human imaging, but also they allow a closer approximation to tumor masses and metastatic sites found in patients. Increasing recent efforts toward developing tumor models, such as hepatocellular carcinomas [4–6], in rats nods to the advantages of using larger animals.

In the study of breast cancer, as in other cancers, developing models for metastatic disease is very important, as it remains the principal cause of mortality. A highly metastatic variant of the commonly used hormone-independent MDA-MB-231 human breast adenocarcinoma was developed by Munoz et al. using serial selection for metastasis in the lungs [7]. This mouse xenograft model, known as 231/LM2-4, was shown to establish macroscopic lung nodules only two months after resection of the primary tumor [7]. In the handful of studies on this tumor model to date, mice have been used exclusively to understand breast tumorigenesis and metastasis [8] and to study the efficacy of anti-

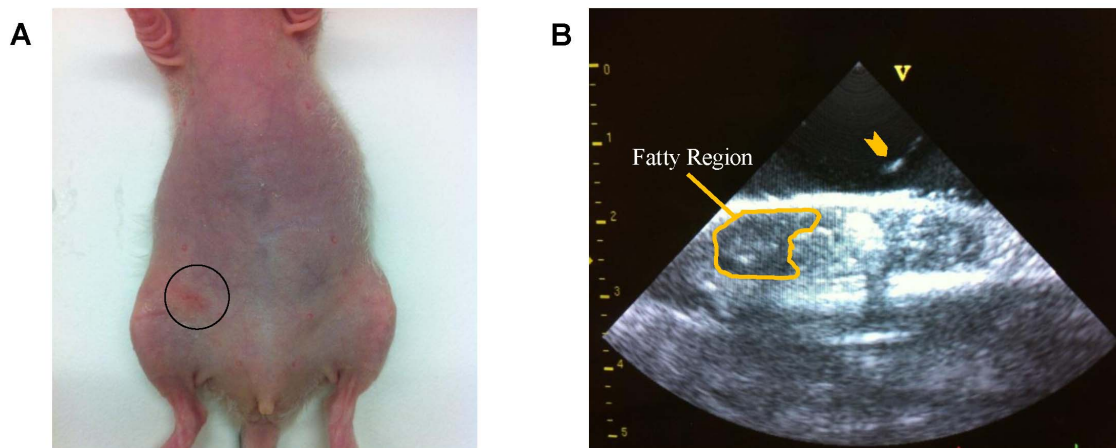


**Figure 1. Cell inoculation under ultrasound image guidance.** (A) Cancer cells were injected through the skin (circle) and into the lower mammary fat pad under ultrasound image guidance. (B) Ultrasound image showing needle tip (arrowhead) and mammary fat pad.  
doi:10.1371/journal.pone.0097950.g001

vascular agents [9]. Establishment of this pro-metastatic variant in a larger animal model has not been reported.

In this study, our aim was to establish the highly metastatic breast cancer xenograft model 231/LM2-4 in nude rats. Using xenografts to mimic breast cancer in rats is not common, and investigations in rats over the past 50 years have been restricted mainly to chemical carcinogenesis [10]. However, commonly used chemical agents such as 7,12-dimethylbenz(a)anthracene (DMBA) or N-nitroso-N-methylurea (NMU) induce mainly hormone-dependent adenocarcinomas [11]. Having the ability to also investigate hormone-independent tumors in rats would be beneficial, in light of the histological similarities that have been demonstrated between rat mammary tumors and human breast cancers [11,12]. In this pilot study, we investigate two different methods for generating xenografts and perform MRI to non-invasively monitor and characterize tumor development in vivo.

## Materials and Methods

### Nude Rats

All procedures were approved by the Hospital for Sick Children Animal Care Committee (protocol #22918) and conducted in accordance with the “Animals for Research Act of Ontario” and “Guidelines of the Canadian Council on Animal Care”. Thirteen healthy 6-weeks-old female immunodeficient rats (Harlan Laboratories) were used in this study, and all efforts were made to minimize distress.

### Tumor Cell Line and Culture

The 231/LM2-4 breast cancer cell line, hereafter referred to as LM2, is a highly metastatic variant of the human adenocarcinoma MDA-MB-231, a triple negative breast cancer (i.e. negative for estrogen receptor, progesterone receptor, and HER2/neu), and was obtained after two rounds of metastasis selection in mice [7]. Cells were grown at 37°C with 5% CO<sub>2</sub> in 1640-RPMI medium (Sigma-Aldrich Canada Inc., Oakville, ON, Canada) supplemented with 10% fetal bovine serum and 0.5% penicillin streptomycin. Fresh supplemented medium was added every other day. Cells were harvested by washing 80% confluent flasks with phosphate buffered saline (PBS) and adding 0.05% trypsin EDTA (Gibco, Carlsbad, CA, USA) to detach cells. Cells were then harvested, counted, and resuspended in PBS at a concentration of  $4 \times 10^7$  cells/mL.

### Tumor Cell Inoculation

Three different methods for establishing xenografts were tested. In one group of rats ( $n=5$ ), cells were prepared in solution containing 25% matrigel (v/v) and approximately  $1 \times 10^7$  cells were injected subcutaneously into the flank. In a second group of rats ( $n=4$ ), approximately  $1 \times 10^7$  cells were injected into the mammary fat pad while the animal was anesthetized with 1.5% isoflurane. A 25G needle was used to minimize trauma to the cells. Injection into the mammary fat pad was performed under real-time ultrasound image guidance, using a GE 10.0FPA 10 MHz pediatric cardiac transducer (GE Healthcare) and a GE VingMed Ultrasound system. Guidance into the fat pad was possible due to strong signal reflection from the needle. Figure 1 shows where the needle was inserted in the rat and how ultrasound image guidance was performed. The needle was placed in the plane of the ultrasound beam and directed at an angle to ensure accurate penetration into the fat pad. This type of image guidance essentially allows one to accurately transplant cells in the desired target without resorting to invasive surgery, which is the standard for orthotopic inoculation. A third group of rats ( $n=4$ ) was also injected orthotopically but without ultrasound image guidance or surgery, thus requiring a certain degree of approximation of the needle penetration depth.

### Magnetic Resonance Imaging

Beginning on Day 6 after cancer cell inoculation, rats were imaged weekly a 3-Tesla clinical MR scanner, using an eight-channel wrist coil for signal detection. Rats were induced on 2% isoflurane in pure oxygen (2 L/min flow rate) and maintained on 1.5% isoflurane during imaging. Rats were placed prone within the coil, resting on top of a water-blanket maintained at 36 degrees Celsius (HTP-1500, Adriot Medical Systems, Loudon, TN, USA). A 24-gauge angiocath was inserted into the lateral tail vein for contrast injection, and this was connected through a 1-mL line tubing to a 3-way stop-cock through which gadolinium (Gd) and saline could be delivered separately. Gd-DTPA (Magnevist, Bayer) was injected as a bolus at a dose of 0.05 mmol/kg, followed by 2 mL of saline.

In addition to localizer scans, a baseline high-resolution anatomical  $T_1$ -weighted spin-echo scan and  $T_1$  map were acquired. The  $T_1$ -weighted spin-echo scan used a 2D acquisition with the following parameters: repetition time (TR) = 724 ms,

echo time (TE) = 14 ms, number of signal averages (NSA) = 3, 100 mm field-of-view (FOV), twenty 1-mm thick slices, and 0.6×0.6 mm in-plane resolution.  $T_1$  mapping consisted of a 3D spoiled fast field echo (T1-FFE) sequence repeated at flip angles of 2°, 10°, and 20°; other parameters were TR = 6.2 ms, TE = 3.2 ms, NSA = 8, 100 mm FOV, twenty 1-mm thick slices, and 0.6×0.6 mm in-plane resolution [13]. A dynamic contrast-enhanced (DCE) MRI sequence was then run to capture the kinetics of contrast uptake and washout. This employed a keyhole acquisition on a 3D T1-FFE to achieve a temporal resolution of 9.1 s while maintaining a spatial resolution of 0.6×0.6×1 mm over twenty slices. This dynamic sequence was run for 8 min and 52 s, and contrast was injected intravenously as a bolus 2 minutes after the start of the dynamic sequence. Immediately afterwards, the  $T_1$ -weighted spin-echo scan and  $T_1$  mapping were repeated.

### Data Analysis

MRI data was transferred to an independent workstation for quantitative data analysis using in-house software developed in Matlab (v.8.1) (MathWorks, Natick, MA).

In-vivo data was first analysed for  $T_1$  relaxation times before contrast injection.  $T_1$  maps were generated by calculating  $T_1$  relaxation times on a pixel-wise basis on every slice in the 3D imaging volume using a previously described method [13]. This allows the conversion of signal intensity at every pixel location to absolute contrast concentration. From the DCE-MRI acquisition, contrast uptake kinetics was then analysed. Based on the calculated baseline  $T_1$  value, the signal intensity time-course at each pixel location was converted to a contrast concentration time-course [14]. The area-under-the-concentration curve was then computed over the first 90 seconds ( $AUC_{90}$ ) after contrast arrival in tissue [15]. The  $AUC_{90}$  metric provides semi-quantitative assessment of the vascularity and leakiness of tumor blood vessels and is a mainstay in current clinical practice of DCE-MRI [16]. To appreciate differences in the contrast uptake profile in different tumor regions, regions-of-interest (ROIs) were drawn to encompass the enhancing tumor rim and low-enhancing core; the ROI-averaged signal intensity  $SI(t)$  was determined as a function of time over the duration of the DCE-MRI acquisition and then expressed as a relative signal enhancement according to the formula,  $SI_{rel}(t) = (SI(t) - SI_{base})/SI_{base} \times 100\%$ , where  $SI_{base}$  is the average pre-injection signal.

### Statistical Analysis

Fisher's exact test (two-tailed) was used to determine if the three methods of cell inoculation were different in their ability to successfully establish tumors. This test is useful when sample sizes are small.

### Histology

Tumors were excised anywhere between 2 to 3 weeks post-tumor induction, depending on their growth rate in vivo. Samples were fixed in 10% neutral buffered formalin at room temperature and processed for histopathology. This involved embedding in paraffin, sectioning into 5  $\mu$ m thick slices, and staining with hematoxylin and eosin (H&E) and CD34. Light microscope images (Olympus BX60) were taken to assess tumor composition, structure, and vascularity.

### Results

#### Successful Establishment of Orthotopic LM2 Tumors in Rats

Tumor induction rate was 100% (4/4) in the orthotopic model when ultrasound image guidance was used and 0% (0/4) when it was not (Table 1). All successfully established tumors demonstrated rapid growth and reached a size of  $1.91 \pm 0.64 \text{ cm}^3$  in 2 to 3 weeks after cell inoculation. This result demonstrates the importance of accurately injecting cells within the mammary fat pad and the effectiveness of ultrasound guidance as a non-invasive alternative to surgery for implanting cells in the fat pad. In contrast, none of the rats injected subcutaneously in the flank (0/5) developed tumors; animals in this group were monitored out to 104 days after cell inoculation (Figure 2), and no evidence of tumor development was visible on imaging or on gross dissection. The three methods of inoculation were different in their ability to successfully establish tumors in vivo ( $p = 0.0028$ ).

#### Magnetic Resonance Imaging

Figure 3 shows in-vivo Gd-enhanced  $T_1$ -weighted spin-echo images in two rats bearing orthotopic LM2 tumors. Rapid induction was consistently observed, with tumors averaging  $0.30 \pm 0.15 \text{ cm}^3$  in size only 6 days after cell inoculation. Growth rate varied, with most tumors reaching critical size (15 mm diameter) by 20 days (Figure 3A) and one tumor reaching critical size after only 13 days (Figure 3B). In all cases, however, enhancement of the tumor upon Gd administration was modest and was restricted mainly to a thin border surrounding the tumor mass.

To quantify DCE-MRI enhancement, Figure 4 superimposes  $AUC_{90}$  maps on anatomical  $T_1$ -weighted spin-echo images and evaluates changes in contrast kinetics as an orthotopic LM2 tumor develops in vivo. Regardless of the stage of tumor progression, the tumor rim always exhibits higher  $AUC_{90}$  values than the tumor core (Figure 4, left column). An important observation, however, is that contrast uptake in the tumor core decreases substantially as the tumor grows in size. This is easily appreciated on signal enhancement profiles over time (Figure 4, middle column). It also

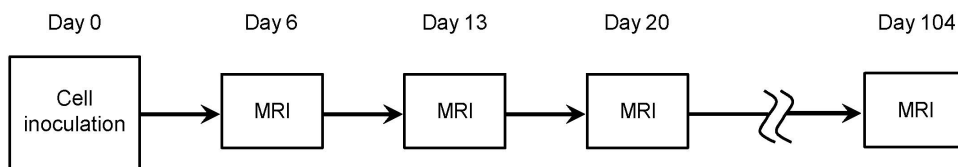


**Figure 2. Experimental design.** Timeline for cell inoculation and magnetic resonance imaging (MRI). doi:10.1371/journal.pone.0097950.g002

**Table 1.** Success of establishing LM2 tumor xenografts in nude rats.

Inoculation method	Take rate	Number of animals
Orthotopic under US* needle guidance	100%	4
Orthotopic without US* needle guidance	0%	4
Subcutaneous (flank)	0%	5

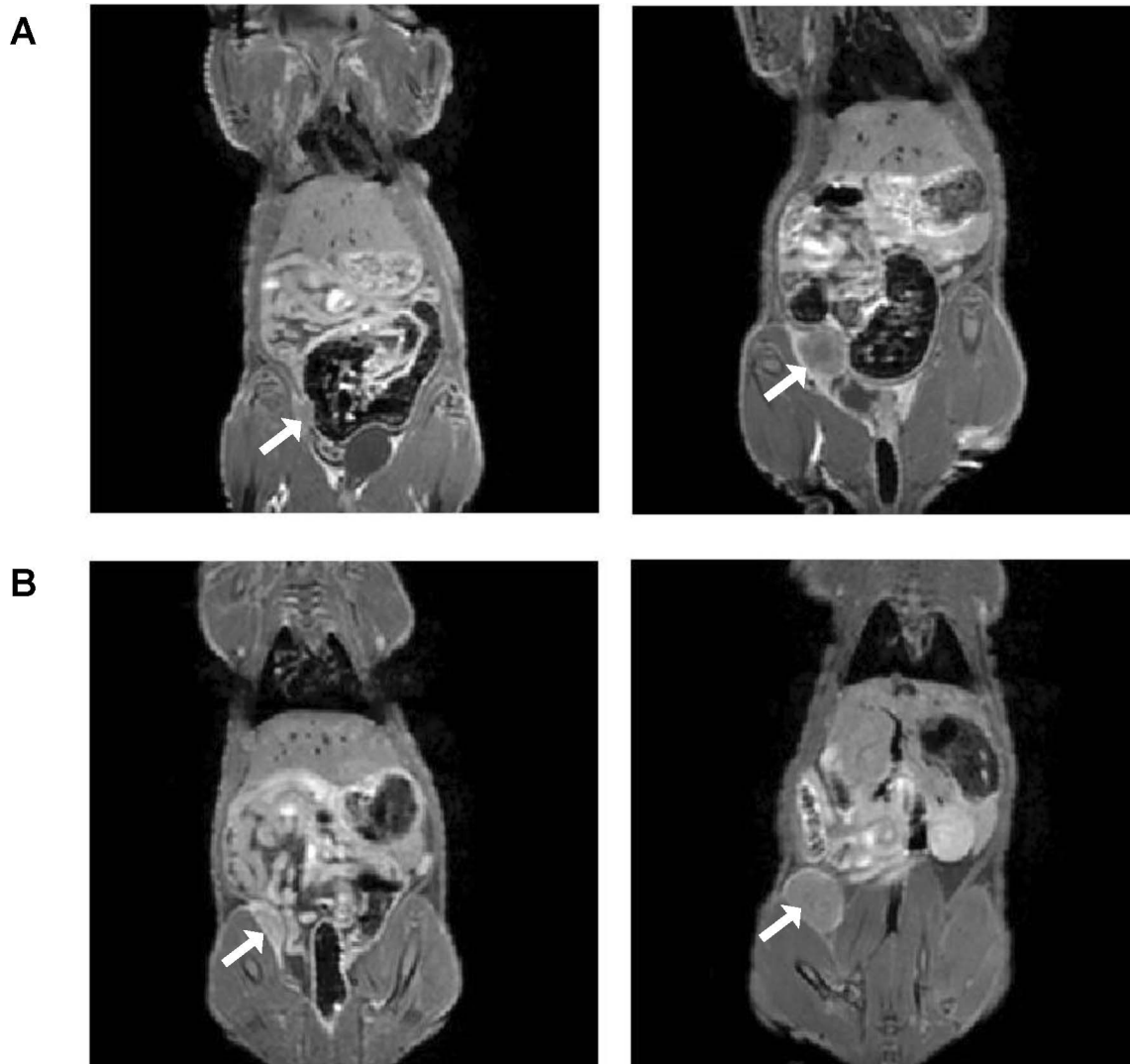
\*US: ultrasound image.  
doi:10.1371/journal.pone.0097950.t001

underlies a shift in the histogram distribution towards very low  $AUC_{90}$  values (Figure 4, right column).

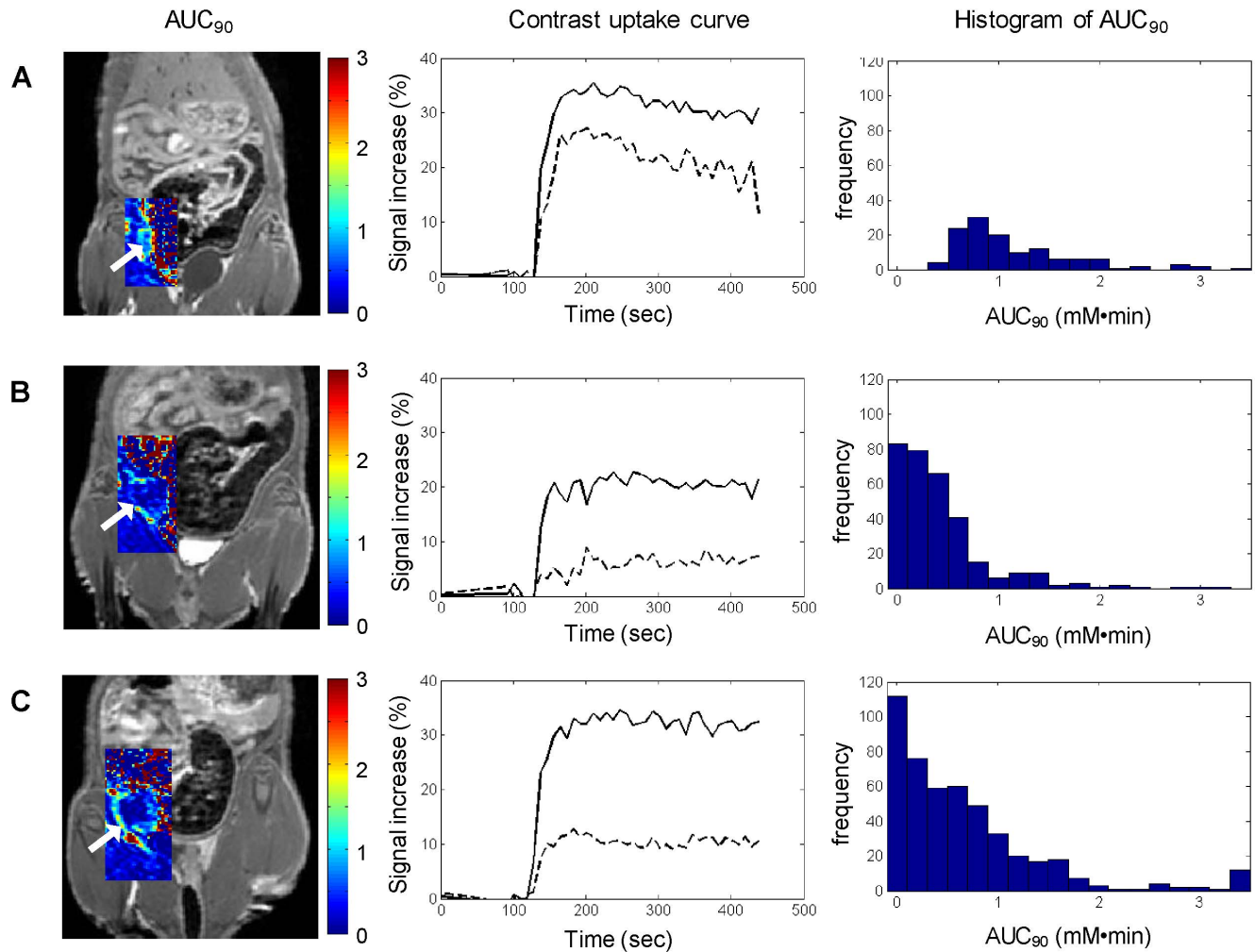
### Histology

Figure 5 shows histological assessment on H&E and CD34. Morphologically, the LM2 tumor presented as a solid mass

comprised of poorly differentiated cancer cells. Very low vascularity was observed and blood vessels that were present were confined mainly to the tumor periphery. Central necrosis was observed in every case and was surrounded by a viable tumor region. In some tumors, completely acellular necrotic areas were also identified.



**Figure 3. In-vivo gadolinium contrast-enhanced magnetic resonance imaging (MRI) of orthotopic breast tumors in nude rats at 3 Tesla.**  $T_1$ -weighted spin-echo images acquired post-contrast injection at early and late stages of tumor development are shown in two rats. (A) MRI was acquired 6 days (left) and 20 days (right) after cell inoculation in the mammary fat pad. (B) MRI was acquired 6 days (left) and 13 days (right) after cell inoculation in the mammary fat pad. Arrow points to tumor.  
doi:10.1371/journal.pone.0097950.g003



**Figure 4. Dynamic contrast-enhanced MRI during tumor progression.** (Left column)  $AUC_{90}$  maps ( $\text{mM}\cdot\text{min}$ ) are overlaid on  $T_1$ -weighted spin-echo images acquired post-contrast injection (A) 6 days, (B) 13 days, and (C) 20 days after cell inoculation in the mammary fat pad. Arrow points to tumor. (Middle column) Corresponding signal enhancement time-course is shown for the tumor rim (solid line) and tumor core (dashed line). (Right column) Corresponding histograms of  $AUC_{90}$  distributions show an evolution toward lower  $AUC_{90}$  values.  
doi:10.1371/journal.pone.0097950.g004

## Discussion

The use of larger animal models such as the nude rat provides tumor burden that more closely resembles human cancer and is therefore invaluable in the development of advanced non-invasive imaging technologies for clinical application. Image spatial resolutions adequate for sensitive detection and detailed delineation in a rat can be translated to imaging metastasis in humans, potentially enabling very early cancer detection of both primary and metastatic lesions. However, although immunodeficient strains have been developed from rats, they are not widely used in cancer studies. In this study, we investigated whether or not the LM2 xenograft model, which is a highly metastatic variant of human adenocarcinoma MDA-MB-231, could be successfully established in nude rats. It was shown that the site of implantation dictated the take rate, with 100% success achieved orthotopically when cell injection into the mammary fat pad was guided by ultrasound and zero success subcutaneously in the flank. MRI monitoring of tumor development *in vivo* demonstrated very rapid progression, with tumors reaching critical size in only 2 to 3 weeks after inoculation. DCE-MRI of Gd contrast kinetics revealed a

hypovascular core that increased in size and decreased in contrast uptake as the tumor grew. Histological assessment on H&E and CD34 revealed low vascularity confined mainly to the tumor rim, which is in agreement with DCE-MRI findings. Central necrosis was also observed, which is consistent with hypoxia as a result of rapid growth and exacerbated by the low vascularity of this tumor model.

The usefulness of the LM2 tumor model is rooted in its highly metastatic nature and the potential to generate spontaneous metastasis in the rat as it does in mice [7]. In this study, we have achieved the important first step of establishing a method to successfully xenograft a primary orthotopic LM2 tumor, which opens the opportunity to study the metastatic process and many aspects of the metastatic cascade that are bypassed using experimental metastasis models (i.e. injecting tumor cells directly to the systemic circulation). The most important advantage of a spontaneous metastasis model is its ability to capture all the early steps in the cascade that are eliminated through experimental metastasis models, including the critical step of how tumor cells break free from the primary site and associate with host cells before residing at distant locations. Due to the rapid growth of the

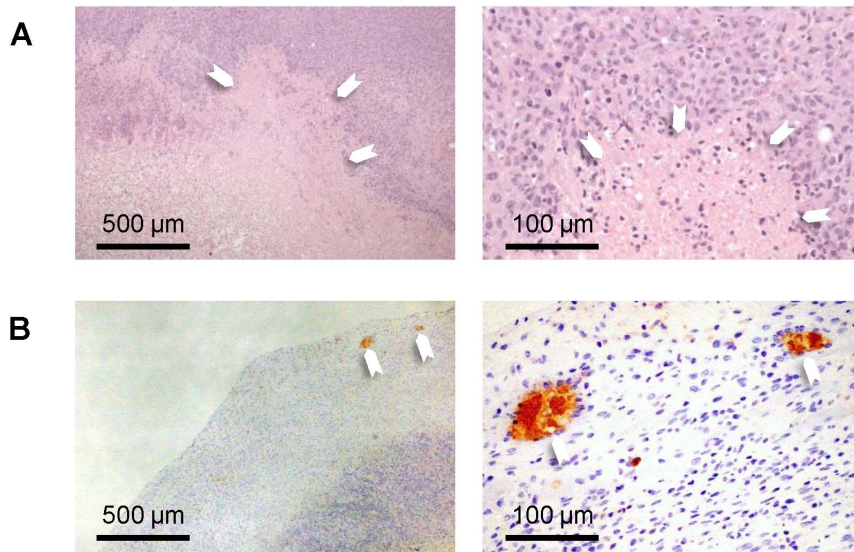


**Figure 5. Histology.** (A) H&E sections reveal poorly differentiated tumor cells and necrotic areas that are partially or completely devoid of cells (arrowheads). (B) CD34 sections show very low vascularity, with blood vessels (arrowheads) confined to the tumor rim. Magnification is  $\times 4$  (left column) and  $\times 20$  (right column).

doi:10.1371/journal.pone.0097950.g005

LM2 model, however, metastasis studies will require complete resection of the primary tumor to control morbidity.

A success rate of 100% for establishing an orthotopic tumor is very high, considering that breast cancer is one of the more difficult tumors to establish in experimental animals, including nude mice and SCID mice, with a success of only 7–20% [17] and considering that take rates are even lower in rats. Further testing in a larger number of rats will establish a more accurate take rate, but we expect this figure would remain high given the results attained in this study. As to the inability of the other two methods to establish tumors, there are plausible explanations. The first method, subcutaneous injections in the flank, is a common approach in mice, and the majority of breast xenograft models in mice are, in fact, subcutaneous. Failure to establish tumors in the rat flank is, therefore, surprising. However, it should be noted that tumor initiation in the flank may not be as rapid as in the mammary fat pad. Where tumor initiation is not rapid, potential differences in immunodeficiency between rats and mice, where it is well known rats are “more leaky”, may result in early elimination of cancer cells by the rat’s own immune response before the tumor has an opportunity to grow. The second method, orthotopic injection, is preferred as the mammary fat pad provides a more favorable microenvironment to rapidly initiate tumor growth. However, with this method it is critical that all the cells are deposited within the fat pad – hence, the need for needle guidance, whether by conventional surgery or non-invasively by ultrasound imaging. When injection is performed without guidance, there is the unwanted possibility that some cells will be deposited outside of the fat pad. Between the two alternatives for needle guidance – surgery versus ultrasound imaging – both require familiarity with the respective techniques, but ultrasound offers the advantage of being completely non-invasive.

MRI and histological findings are consistent. Together, they demonstrate a rapidly progressing tumor characterized by very low vascularity confined to the rim and an expanding central necrotic region in which Gd uptake, as measured by  $AUC_{90}$ , decreases as the tumor grows. There are multiple influences on the uptake of Gd, the primary ones being vascularity and blood vessel

leakiness. Therefore, areas with high  $AUC_{90}$  correspond to areas where blood vessels are present to deliver Gd to the tumor. However, Gd is an extravascular contrast agent, meaning that it will extravasate from blood vessels and flow into the interstitial space. The transport of Gd through the interstitium is dictated by its own concentration gradient and also by interstitial fluid pressure. If high interstitial fluid pressure is present in the tumor core, the transport of Gd will be slow and will result in low  $AUC_{90}$  values. Gross dissection revealed a fluid-filled core in some tumors, which is consistent with high interstitial fluid pressure. This area corresponds both to the low  $AUC_{90}$  region on MRI and to the necrotic region on histology. Overall, the MRI and histological findings demonstrate that the LM2 is an orthotopic breast tumor model that requires little vascular support and yet can maintain rapid growth.

Future studies will investigate spontaneous metastasis arising from a primary LM2 breast tumor. The primary lesion will be removed 2 to 3 weeks after inoculation, depending on the growth rate *in vivo*, and the animal recovered. It is expected that successful xenografts will be established most of the time, given the high take rate achieved in this study. The time to appearance of metastatic lesions will need to be determined and may likely differ from the two months interval reported in mice [7]. These studies will provide a platform for developing and applying new MRI methods for investigating and detecting breast cancer metastasis.

## Conclusions

This study established for the first time in nude rats a highly metastatic orthotopic breast cancer known as LM2. It was shown that success was highly dependent on the site of inoculation, with the orthotopic site yielding 100% take rate while the subcutaneous (flank) site failed to produce xenografts. Monitoring by contrast-enhanced MRI revealed rapid growth *in vivo* and low uptake of exogenously administered Gd. Assessment on histology demonstrated findings consistent with imaging, including low vascularity confined to the tumor rim and a rapidly developing necrotic core. Establishment of this tumor model lays the foundation for studying

spontaneous metastasis models of breast cancer in a larger rat model.

## Acknowledgments

We thank Bernard Castro and Huimin Wang for histology; Tameshwar Ganesh, Mosa Alhamami, and Reza Mokhtari for microscopy work; and Dr. Adam Waspe for helpful advice on ultrasound image needle guidance.

## References

- Olsen OE (2013) Advances in pediatric oncology MRI. *Acta Radiol* 54: 1030–1036.
- Lederle W, Palmowski M, Kiessling F (2012) Imaging in the age of molecular medicine: monitoring of anti-angiogenic treatments. *Curr Pharm Biotechnol* 13: 595–608.
- Dickinson L, Ahmed HU, Allen C, Barentsz JO, Carey B, et al. (2013) Scoring systems used for the interpretation and reporting of multiparametric MRI for prostate cancer detection, localization, and characterization: could standardization lead to improved utilization of imaging within the diagnostic pathway? *J Magn Reson Imaging* 37: 48–58.
- Thompson SM, Callstrom MR, Knudsen B, Anderson JL, Butters KA, et al. (2013) AS30D model of hepatocellular carcinoma: tumorigenicity and preliminary characterization by imaging, histopathology, and immunohistochemistry. *Cardiovascular and interventional radiology* 36: 198–203.
- Guo Y, Klein R, Omary RA, Yang GY, Larson AC (2011) Highly malignant intra-hepatic metastatic hepatocellular carcinoma in rats. *Am J Transl Res* 3: 114–120.
- Chan HH, Chu TH, Chien HF, Sun CK, Wang EM, et al. (2010) Rapid induction of orthotopic hepatocellular carcinoma in immune-competent rats by non-invasive ultrasound-guided cells implantation. *BMC gastroenterology* 10: 83.
- Munoz R, Man S, Shaked Y, Lee CR, Wong J, et al. (2006) Highly efficacious nontoxic preclinical treatment for advanced metastatic breast cancer using combination oral UFT-cyclophosphamide metronomic chemotherapy. *Cancer Res* 66: 3386–3391.
- Medina-Ramirez CM, Goswami S, Smirnova T, Bamira D, Benson B, et al. (2011) Apoptosis inhibitor ARC promotes breast tumorigenesis, metastasis, and chemoresistance. *Cancer Res* 71: 7705–7715.
- Daenen LG, Shaked Y, Man S, Xu P, Voest EE, et al. (2009) Low-dose metronomic cyclophosphamide combined with vascular disrupting therapy induces potent antitumor activity in preclinical human tumor xenograft models. *Mol Cancer Ther* 8: 2872–2881.
- Huggins C, Grand LC, Brillantes FP (1961) Mammary cancer induced by a single feeding of polymucular hydrocarbons, and its suppression. *Nature* 189: 204–207.
- Russo J, Russo IH (2000) Atlas and histologic classification of tumors of the rat mammary gland. *J Mammary Gland Biol Neoplasia* 5: 182–200.
- Russo J, Gusterson BA, Rogers AE, Russo IH, Wellings SR, et al. (1990) Comparative study of human and rat mammary tumorigenesis. *Lab Invest* 62: 244–278.
- Cheng HL, Wright GA (2006) Rapid high-resolution T(1) mapping by variable flip angles: accurate and precise measurements in the presence of radiofrequency field inhomogeneity. *Magn Reson Med* 55: 566–574.
- Cheng HL (2008) Investigation and optimization of parameter accuracy in dynamic contrast-enhanced MRI. *J Magn Reson Imaging* 28: 736–743.
- Cheng HL (2009) Improved correlation to quantitative DCE-MRI pharmacokinetic parameters using a modified initial area under the uptake curve (mIAUC) approach. *J Magn Reson Imaging* 30: 864–872.
- Punwani S (2011) Contrast enhanced MR imaging of female pelvic cancers: established methods and emerging applications. *European journal of radiology* 78: 2–11.
- Mehta RR, Graves JM, Hart GD, Shilkaitis A, Das Gupta TK (1993) Growth and metastasis of human breast carcinomas with Matrigel in athymic mice. *Breast Cancer Res Treat* 25: 65–71.

## Author Contributions

Conceived and designed the experiments: JN HLC. Performed the experiments: JN HLC. Analyzed the data: HLC. Contributed reagents/materials/analysis tools: HLC. Wrote the paper: HLC.